

A singlet doublet dark matter model with radiative neutrino masses

Sonja Esch^a, Michael Klasen^a, Carlos E. Yaguna^b

^a*Institut für Theoretische Physik, Westfälische Wilhelms-Universität Münster, Wilhelm-Klemm-Straße 9, D-48149 Münster, Germany*

^b*Universidad Pedagógica y Tecnológica de Colombia at Sede Central Tunja-Bayacá-Colombia, Avenida Central del Norte 39-115*

E-mail: sonja.esch@uni-muenster.de, michael.klasen@uni-muenster.de,
cyaguna@gmail.com

ABSTRACT: We present a detailed study of a combined singlet-doublet scalar and singlet-doublet fermion model for dark matter. These models have only been studied separately in the past. We show that their combination allows for the radiative generation of neutrino masses, but that it also implies the existence of lepton-flavour violating (LFV) processes. We first analyse the dark matter, neutrino mass and LFV aspects separately. We then perform two random scans for scalar dark matter imposing Higgs mass, relic density and neutrino mass constraints, one over the full parameter space, the other over regions where scalar-fermion coannihilations become important. In the first case, a large part of the new parameter space is excluded by LFV, and the remaining models will be probed by XENONnT. In the second case, direct detection cross sections are generally too small, but a substantial part of the viable models will be tested by future LFV experiments. Possible constraints from the LHC are also discussed.

KEYWORDS: Minimal models, dark matter, neutrino masses, lepton flavour violation

Contents

1	Introduction	1
2	Particle content and interactions in the model	3
3	Dark matter relic density	5
4	Neutrino masses	9
5	Lepton flavour violation	13
6	Numerical results	14
6.1	Random scan	16
6.2	Coannihilation region	17
6.3	LHC constraints	19
7	Conclusion	22

1 Introduction

While the Standard Model (SM) is certainly a highly successful theory of particle physics and, with the discovery of a Higgs-like boson by the ATLAS [1] and CMS [2] experiments at the CERN Large Hadron Collider (LHC) in 2012, is sometimes presented as complete, it is generally believed to suffer from conceptual and phenomenological deficiencies. Important examples are the unexplained large hierarchy of interactions [3, 4], the surprisingly small, but non-zero masses of neutrinos [5] established first in 1998 by the oscillations of atmospheric [6], then of solar [7, 8] and reactor neutrinos [9], and the observational evidence from many different scales [10] for a sizeable dark matter density in the Universe, quantified by WMAP [11] and then, more precisely, by the Planck satellite [12] to be $\Omega^{\text{obs}} h^2 = 0.1186 \pm 0.0031$. Here, h denotes the present Hubble expansion rate in units of $100 \text{ km s}^{-1} \text{ Mpc}^{-1}$.

An intriguing remedy for these problems is to extend the SM minimally by a small number (≤ 4) of new scalar and fermion fields, which allow to generate small neutrino masses radiatively and which have one (or more) neutral components that could represent dark matter. One of the most popular so-called radiative seesaw models is the scotogenic model with only one additional scalar (inert Higgs) $SU(2)_L$ doublet and a (right-handed neutrino) fermion singlet [13], for which we recently demonstrated the importance of coannihilations between the scalar dark matter and the right-handed neutrinos [14]. Many variants with general N -tuplets containing in general two scalars and one fermion have subsequently been proposed [15–18]. The new fields are usually assumed to be odd under a Z_2 symmetry to

stabilize the dark matter and (in some cases) to prevent tree-level contributions to neutrino masses. All one-loop models connecting neutrino masses to dark matter with at most four additional fields have been classified [19] following the notation of a systematic study of the $d = 5$ Weinberg operator at one-loop order [20]. The classification has recently been extended to two loops [21] following Ref. [22] (cf. also Sec. 4.7 in [23]).

Apart from the models mentioned above, which all belong to the one-loop topology T3 as defined in Refs. [19, 20], several models with other topologies have also been studied in the past. They include a model of topology T1-1 with three scalars, two of which are equivalent, and one fermion [24], and a model of topology T1-3 with one scalar and three fermions [25–27]. In both cases, the lightest scalar was assumed to represent the dark matter, constraints from the Higgs and neutrino sectors and the relic density were imposed, and their phenomenology, in particular of lepton-flavour violating processes, has been studied. In this paper, we study a model of topology T1-2 with two scalars and two fermions. A general discussion of this topology, without establishing the particle content of specific models, has been presented in Ref. [28]. To complete the list, note that models of topology T2 can be discarded on dimensional arguments, while models of T4, T5 and T6 always have tree-level contributions to neutrino masses and thus no obvious connection to dark matter. In addition, three out of six models of type T4 and all models of type T5 and T6 are divergent at one loop.

As mentioned above, we study in this paper a model of topology T1-2 with two scalars and two fermions. We focus on the first of these models, T1-2-A in the classification of Ref. [19], with a singlet Majorana fermion ψ_S of hypercharge parameter $\alpha = 0$, that determines also the hypercharges of the vector-like fermion doublet ψ_D , the singlet scalar ϕ_S , and the complex doublet scalar ϕ_D . The alternative case $\alpha = -2$, called the Inert Zee Model, has previously been analysed and found to be consistent with constraints from neutrino oscillation, dark matter and lepton-flavour violation data [29]. A doublet-triplet model, T1-2-F with $\alpha = -1$, has also been analysed in a similar way [30]. Since our model T1-2-A with $\alpha = 0$ is equivalent to T1-2-C with $\alpha = -1$, our results equally apply to this model. It is furthermore one of the models, together with the model T1-3-A and $\alpha = 0$ [25–27], that allows for gauge coupling unification at a scale $\Lambda = \mathcal{O}(10^{13})$ GeV, at variance with most of the other models mentioned above including the original scotogenic model [31].

The paper is organised as follows: In Sec. 2 we define our model by describing its particle content, mass and interaction Lagrangians, free parameters and particle mixings. In Sec. 3 we review the implications for the dark matter relic density first of the scalar and fermion sectors separately, before we study the new regions of parameter space that open up when they couple to each other as required for neutrino mass generation. The latter is discussed in Sec. 4 in analytic and numerical form using a Casas-Ibarra parameterisation and limits of small couplings. As lepton-flavour violation always occurs in this type of models, we compute the branching ratios for $\mu \rightarrow e\gamma$ and similar processes in Sec. 5. Sec. 6 contains our main numerical results from two random scans, one over the full parameter space, one in the coannihilation region of scalars and fermions. We impose all current experimental constraints, estimate the sensitivity of future experiments and discuss the possible impact of the LHC. Our conclusions are given in Sec. 7.

2 Particle content and interactions in the model

In our model T1-2-A, the SM is extended by two scalars, a real singlet ϕ_S and a complex doublet ϕ_D , and two fermions, a Weyl singlet ψ_S and a vector-like doublet ψ_D , which can be decomposed into two chiral Weyl fermions ψ_{D_1}, ψ_{D_2} . The new (SM) particles are all assumed to be odd (even) under a discrete Z_2 symmetry to render dark matter stable and generate neutrino masses only at the loop level. Under the combined $SU(2)_L \otimes U(1)_Y \otimes Z_2$ symmetry group, the new particles carry the quantum numbers

$$\phi_S \propto (1, 0, -), \quad \phi_D = \begin{pmatrix} \phi^+ \\ \phi_R + i\phi_I \end{pmatrix} \propto (2, \frac{1}{2}, -) \quad (2.1)$$

$$\psi_S \propto (1, 0, -), \quad \psi_{D_1} = \begin{pmatrix} \psi_{D_{1,L}}^0 \\ \psi_{D_{1,L}}^- \end{pmatrix} \propto (2, -\frac{1}{2}, -), \quad \psi_{D_2} = \begin{pmatrix} -(\psi_{D_{2,R}}^-)^\dagger \\ (\psi_{D_{2,R}}^0)^\dagger \end{pmatrix} \propto (2, \frac{1}{2}, -). \quad (2.2)$$

The pair of Weyl fermions are required for the cancellation of anomalies. For the doublets, the decompositions according to the physical charges $Q = T_3 + Y/2$ have also been indicated. It is evident that the model can be seen as a combination of the singlet-doublet scalar [32–35] and the singlet-doublet fermion dark matter model [32, 33, 36–38], which have both well been studied separately. Our model allows in addition for the radiative generation of neutrino masses.

The Lagrangian of the singlet-doublet scalar model

$$\begin{aligned} -\mathcal{L}_{\text{scalar}} = & \frac{1}{2}\lambda_S\phi_S^2|H|^2 + \lambda_D|\phi_D|^2|H|^2 + \lambda'_D|\phi_D^\dagger H|^2 + \frac{1}{2}\lambda_D''\left[\left(\phi_D^\dagger H\right)^2 + \text{h.c.}\right] \\ & + A\left[\phi_D^\dagger H\phi_S + \text{h.c.}\right] + \frac{1}{2}M_{S,S}^2\phi_S^2 + M_{D,S}^2|\phi_D|^2 \end{aligned} \quad (2.3)$$

involves in general five different couplings of the new scalars with the complex SM Higgs doublet H , which acquires a vacuum expectation value $v = 246$ GeV and thus breaks the electroweak symmetry. One of these couplings (A) links the singlet and doublet scalars with the SM Higgs in a Yukawa-like form. The Z_2 symmetry remains unbroken, *i.e.* the new scalars do not have quartic potentials and do not acquire a vacuum expectation value, but have explicit mass terms. The Lagrangian of the singlet-doublet fermion model

$$-\mathcal{L}_{\text{fermion}} = y_1\psi_{D_1}H\psi_S + y_2\psi_{D_2}H^\dagger\psi_S + \frac{1}{2}M_{S,F}\psi_S^2 + M_{D,F}\psi_{D_1}\psi_{D_2} + \text{h.c.} \quad (2.4)$$

contains a Majorana mass term for the singlet ψ_S , a Dirac mass term for the doublet ψ_D as well as two Yukawa terms connecting the singlet and doublet fermions with the SM Higgs. The presence of scalar and fermion singlets and doublets allows also to define couplings of the new particles to the SM leptons,

$$-\mathcal{L}_{\text{lepton}} = g_{1i}L_i\phi_S\psi_{D_2} + g_{2i}L_i\phi_D\psi_S + \text{h.c.}, \quad (2.5)$$

where

$$L_i = \begin{pmatrix} \nu_{i,L}^0 \\ e_{i,L}^- \end{pmatrix} \propto (2, -\frac{1}{2}, +) \quad (2.6)$$

Table 1. Free parameters in model T1-2-A.

Sector	Parameters
Scalar sector	$M_{S,S}, M_{D,S}, \lambda_S, \lambda_D, \lambda'_D, \lambda''_D, A$
Fermion sector	$M_{S,F}, M_{D,F}, y_1, y_2$
Neutrino sector	$g_{11}, g_{12}, g_{13}, g_{21}, g_{22}, g_{23}$

is the SM lepton doublet of generation i . These new Yukawa couplings g_{ij} allow to obtain one-loop neutrino masses after electroweak symmetry breaking, while at tree level the neutrinos remain massless. A term $g_{3i}e_{i,R}^c\phi_D^\dagger\psi_{D1}$ with no effect on neutrino masses has been omitted. The presence of these non-zero neutrino masses implies lepton flavour violation. Inspection of Eqs. (2.3)–(2.5) shows that the terms featuring A , y_1 , y_2 and g_{ij} do not allow to determine the lepton numbers of the new particles consistently without violating lepton flavour. Only when either g_{ij} or all mixing terms A , y_1 and y_2 vanish, lepton flavour symmetry can be restored.

In the basis of real neutral scalars (ϕ_S, ϕ_R, ϕ_I) , one can extract their mass matrix after electroweak symmetry breaking from the Lagrangian in Eq. (2.3) [33]

$$M_{\text{scalar}}^2 = \begin{pmatrix} M_{S,S}^2 + \frac{1}{2}v^2\lambda_S & Av & 0 \\ Av & M_{D,S}^2 + \frac{1}{2}v^2(\lambda_D + \lambda'_D + \lambda''_D) & 0 \\ 0 & 0 & M_{D,S}^2 + \frac{1}{2}v^2(\lambda_D + \lambda'_D - \lambda''_D) \end{pmatrix}. \quad (2.7)$$

In the absence of new sources of CP-violation, ϕ_I does not mix with either ϕ_R or ϕ_S . The mass matrix for the neutral fermions can similarly be derived from the Lagrangian in Eq. (2.4) [33], so that

$$M_{\text{fermion}} = \begin{pmatrix} M_{S,F} & m_y \cos \theta & m_y \sin \theta \\ m_y \cos \theta & 0 & M_{D,F} \\ m_y \sin \theta & M_{D,F} & 0 \end{pmatrix}. \quad (2.8)$$

Here, $m_y = \frac{1}{\sqrt{2}}yv$ with $y = \sqrt{y_1^2 + y_2^2}$, v is the SM Higgs vacuum expectation value, and $\tan \theta = \frac{y_2}{y_1}$, so that $y_1 = y \cos \theta$ and $y_2 = y \sin \theta$. Mixing of the neutral scalar and fermion particles is parameterized by the matrices U_S and U_F , which leads to the mass eigenstates

$$\begin{pmatrix} X_1 \\ X_2 \\ X_3 \end{pmatrix} = U_S \begin{pmatrix} \phi_S \\ \phi_R \\ \phi_I \end{pmatrix}, \quad \begin{pmatrix} \chi_1 \\ \chi_2 \\ \chi_3 \end{pmatrix} = U_F \begin{pmatrix} \psi_S \\ \psi_{D1}^0 \\ \psi_{D2}^0 \end{pmatrix}. \quad (2.9)$$

Due to the mixing with ψ_S , all physical fermions χ_i are Majorana particles. In addition to the neutral sector, one obtains a charged scalar ϕ_D^- with mass $m_{\phi_D^-}$ and a charged fermion

$$\chi^- = \begin{pmatrix} D_{1,L}^- \\ D_{2,R}^- \end{pmatrix} \quad (2.10)$$

with mass $m_{\psi^-} = M_{D,F}$. In total, our model contains 17 free parameters, which are summarized in Tab. 1.

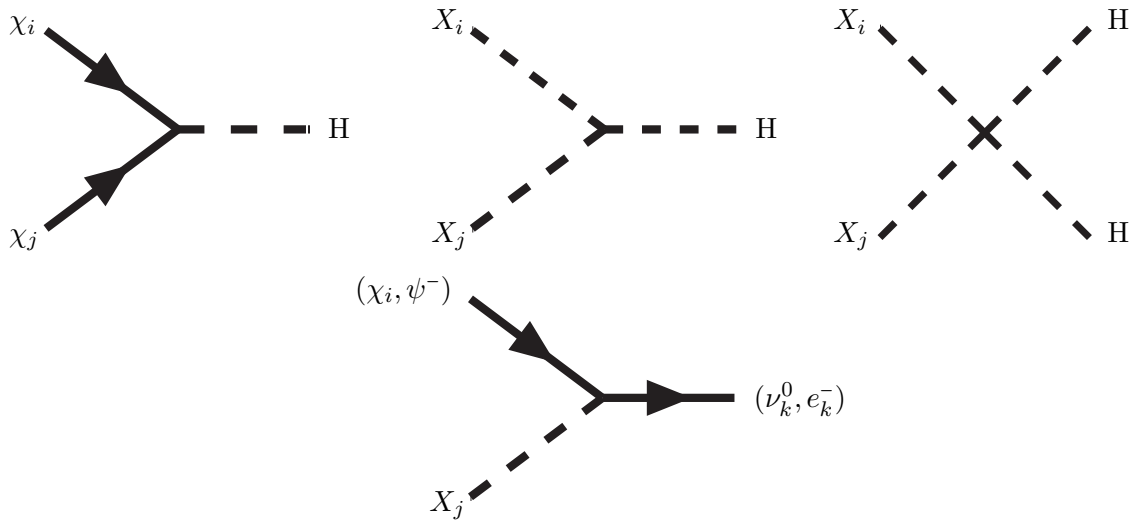


Figure 1. New vertices that link the Z_2 -odd sector to the Standard Model.

3 Dark matter relic density

Let us first review the fermion and scalar dark matter sectors of our model separately. The singlet-doublet fermion model has been shown to be severely constrained by LUX and XENON1T. Only regions with small Yukawa coupling $y < 0.1$ are still allowed, and those are fine-tuned to at least 10%. The singlet-doublet scalar model was less constrained by LUX. In the limit $\lambda = \lambda_S = \lambda_D$ with $\lambda'_D = \lambda''_D = 0$, regions of $\lambda < 0$ were, however, excluded by XENON1T, while $\lambda > 0$ remained viable, albeit again with a typical fine-tuning of $\leq 10\%$ [33]. The correct relic density is reached in a thermal freeze-out through electroweak interactions and often through resonances or via coannihilation processes [32]. In both cases, the dark matter mass had to be in the few hundred GeV to few TeV range. Relic density and direct detection constraints are correlated through the same Higgs couplings, shown in the top row of Fig. 1. We have verified that we correctly reproduce the results in Ref. [33] separately for fermion and scalar singlet-doublet dark matter.

Our model allows for both fermion and scalar dark matter candidates as well as for fermion-scalar coannihilation processes, mediated by the lepton vertex shown in the bottom row of Fig. 1. This implies also that our dark sector can be leptophilic, if the Higgs couplings are small, and that new annihilation processes, shown in Fig. 2, can occur, which will in general relax the correlation of relic density and direct detection constraints via the Higgs couplings. The annihilation cross sections of these processes scale with the relative velocity v of the thermal relic as

$$\sigma v(\chi_i \chi_j \rightarrow e_k^+ e_l^-) \propto v^2 \quad , \quad \sigma v(X_i X_j \rightarrow e_k^+ e_l^-) \propto v^4, \quad (3.1)$$

$$\sigma v(\chi_i \chi_j \rightarrow \nu_k^0 \nu_l^0) \propto v^0 \quad , \quad \sigma v(X_i X_j \rightarrow \nu_k^0 \nu_l^0) \propto v^2, \quad (3.2)$$

respectively. Conversion processes $\chi_i \chi_j \leftrightarrow X_k X_l$ can also occur, so that the evolution of the dark matter particle is described by a set of coupled Boltzmann equations. We solve these with micrOMEGAs 4.0.3 [39] after implementation of the Lagrangians in Eqs. (2.3)–(2.5)

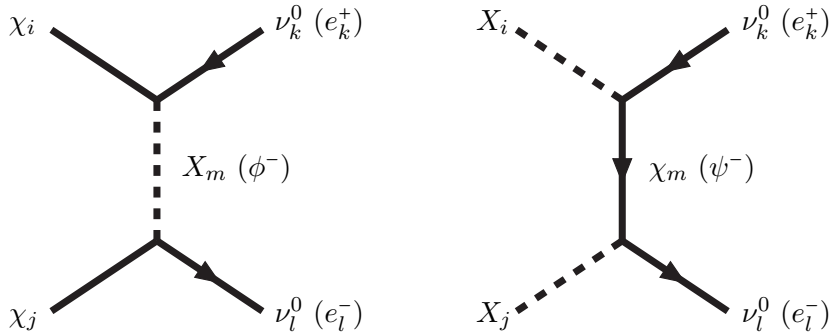


Figure 2. (Co-)annihilation processes of fermion (left) and scalar (right) dark matter particles to SM leptons.

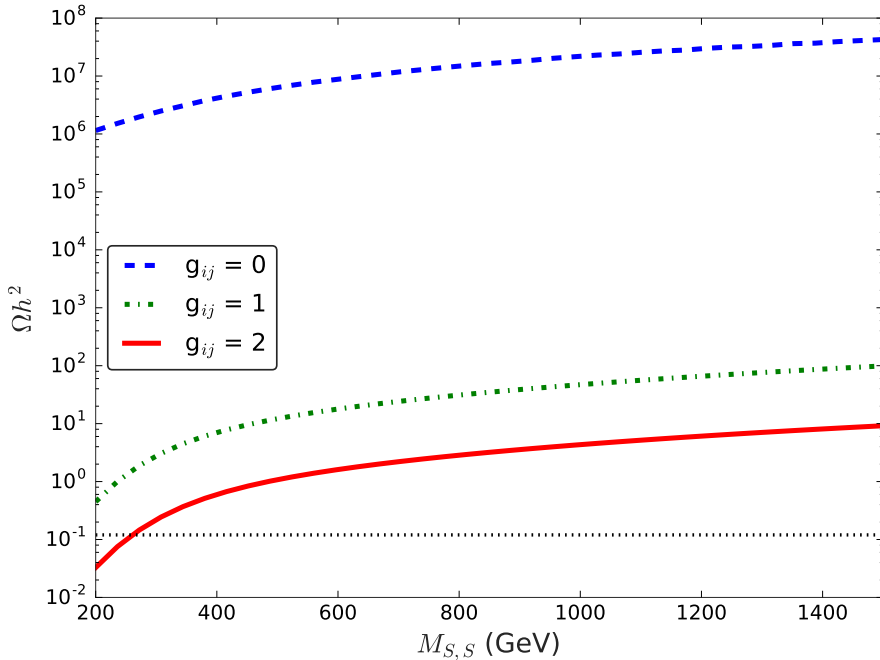


Figure 3. Influence of the scalar-fermion couplings g_{ij} on the singlet scalar dark matter relic density as a function of its mass parameter $M_{S,S}$.

in LanHEP [40] and SARAH 4 [41] as a cross-check and to facilitate use of the spectrum generator SPheno 3.3.6 [42].

In Fig. 3, we demonstrate the impact of the couplings g_{ij} among the new fermion and scalar sectors on the singlet scalar dark matter relic density as function of its mass. The other masses $M_{D,S}$, $M_{S,F}$ and $M_{D,F}$ are scaled to it and larger by factors of 3, 3.1 and 2.5, respectively, so that coannihilations are unimportant. Mixings and (co-)annihilations

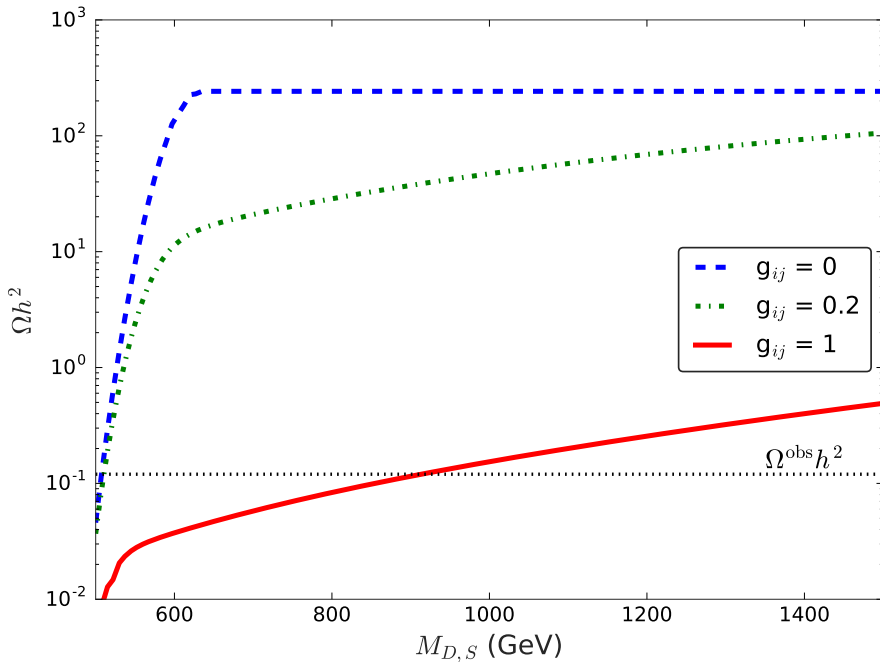


Figure 4. Influence of the scalar-fermion couplings g_{ij} on the singlet fermion dark matter relic density as function of the doublet scalar mass parameter $M_{D,S}$.

in the scalar sector alone are further suppressed by small scalar couplings λ_S etc., which are all set to values below 10^{-5} , so that the relic density with $g_{ij} = 0$ (dashed blue line) is seven orders of magnitude larger than the value observed by Planck (dotted black line). Increasing the scalar-fermion coupling to $g_{ij} = 2$ (full red line) then allows to bring the singlet scalar relic density in agreement with the observation, whereas $g_{ij} = 1$ (dot-dashed green line) is not quite sufficient. The direct detection cross section is independent of g_{ij} , so that it can be decoupled from the relic density constraint.

Next, we consider the effect of the couplings g_{ij} on singlet fermion dark matter. Fig. 4 shows its relic density as a function of the doublet scalar mass $M_{D,S}$. The singlet and doublet fermion masses have been fixed at $M_{S,F} = 450$ GeV and $M_{D,F} = 3$ TeV, respectively, and the singlet scalar mass is 2.5 TeV, so that dark matter is always fermionic in the mass range shown. Since the Yukawa couplings $y_1 = 0.06$ and $y_2 = 0.28$ are small, it is also dominated by the singlet component. In the absence of scalar-fermion couplings g_{ij} (dashed blue line), the relic density stays constant above $M_{D,S} = 600$ GeV. Below this value, the mass difference of the lightest physical scalar and fermion falls to a few tens of GeV and conversion processes $\chi_i \chi_j \leftrightarrow X_k X_l$ can occur, which depletes the relic density to acceptable values when $M_{D,S} \simeq M_{S,F}$. When the scalar-fermion couplings are set to $g_{ij} = 0.2$ (dot-dashed green line) or even to $g_{ij} = 1$ (full red line), the relic density falls monotonically with the doublet scalar mass, as coannihilations become more and more important. Even for large values of $M_{D,S}$, the relic density is smaller than for $g_{ij} = 0$ due

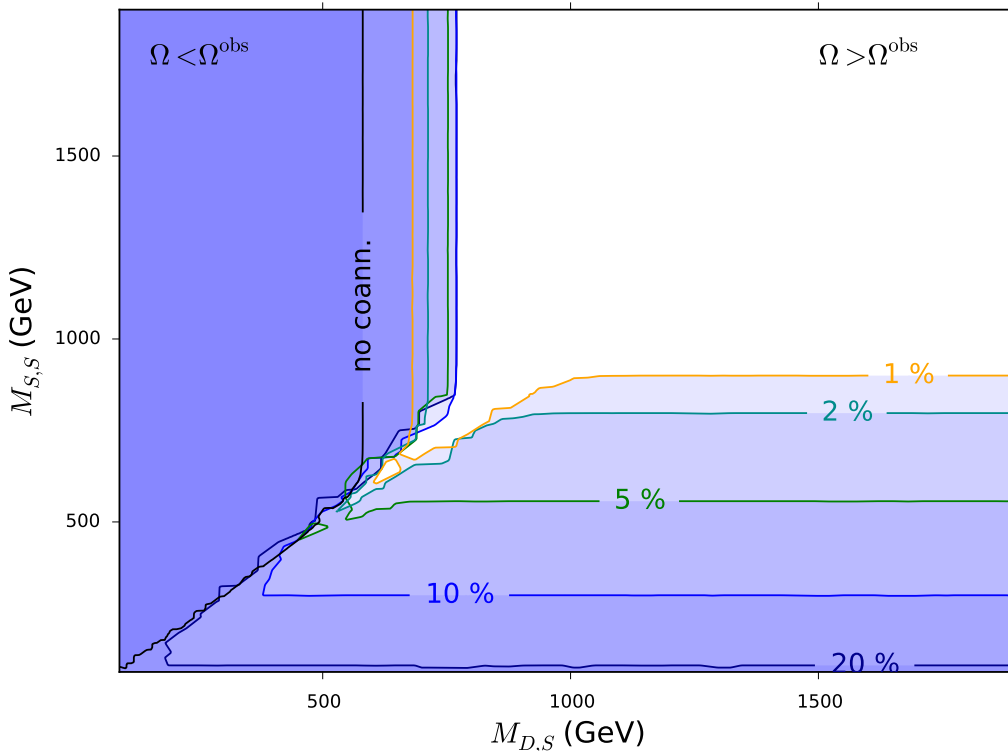


Figure 5. Viable and excluded values of the scalar dark matter relic density in the mass plane $M_{D,S}$ – $M_{S,S}$ in the presence of similarly light singlet or doublet fermions with couplings $g_{ij} = 0.75$.

to the presence of additional annihilation channels into SM neutrinos and charged leptons (see Fig. 2 left). Their effect becomes smaller due to the scalar propagator suppression as $M_{D,S}$ increases. The direct detection cross section is, of course, again independent of g_{ij} .

In Fig. 5, we analyse the scalar dark matter relic density in the mass plane $M_{D,S}$ – $M_{S,S}$ in the presence of similarly light singlet or doublet fermions for a fixed, sizeable value of $g_{ij} = 0.75$. The scalar couplings are either small ($\lambda_S = \lambda'_D = 10^{-4}$, $A = 10^{-4}$ GeV) or zero ($\lambda_D = \lambda'_D = 0$), so that the dark matter particle is mostly a singlet when $M_{S,S} < M_{D,S}$ and a doublet when $M_{D,S} < M_{S,S}$. The Yukawa couplings have been set to $y_1 = 0.3$ and $y_2 = 0.2$, respectively. When the fermions are decoupled to $M_{S,F} = M_{D,F} = 5$ TeV (full black line), coannihilations cannot take place, and one recovers the result in Fig. 12 of Ref. [33]. However, when the relative mass difference of singlet fermions to doublet scalars is in the few-percent range (coloured vertical lines), the allowed range in the relic density is extended beyond $M_{D,S} = 600$ GeV to about 750 GeV. Conversely, when the relative mass difference of doublet fermions to singlet scalars is in the few-percent range (coloured horizontal lines), a new region of singlet scalar dark matter opens up due to scalar-fermion coannihilations, conversion processes and annihilations into SM leptons. For relative mass differences of 1–10%, the singlet scalar dark matter mass cannot exceed 900 and 250 GeV, respectively.

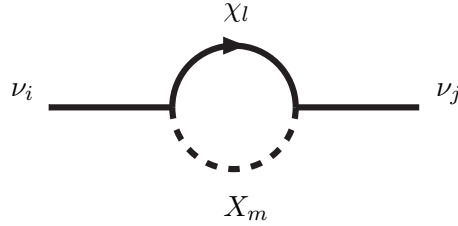


Figure 6. Neutrino-mass generation at one loop in model T1-2-A after electroweak symmetry breaking.

4 Neutrino masses

The combination of a singlet-doublet scalar and a singlet-doublet fermion sector in model T1-2-A allows for the radiative generation of neutrino masses through the box diagram depicted in Fig. 2 of Ref. [19] and thus for a natural explanation of the small relative size of neutrino masses with respect to other fermion masses. Radiative neutrino mass models have been reviewed extensively in Ref. [23] including both radiative Dirac and Majorana mass schemes. The latter can be classified according to the loop-order realization of the Weinberg operator. Here, we focus on the one-loop realization of the $d = 5$ operator [20].

After electroweak symmetry breaking, Majorana neutrino masses in our model are generated at one loop by the diagram shown in Fig. 6. The neutrino mass matrix is then given by

$$M_{\nu,ij} = \sum_{l,m} \frac{1}{16\pi^2} \frac{M_{\chi_l}}{M_{X_m}^2 - M_{\chi_l}^2} \left(M_{\chi_l}^2 \ln M_{\chi_l}^2 - M_{X_m}^2 \ln M_{X_m}^2 \right) \left[U_{F,3l}^2 U_{S,1m}^2 g_{1i} g_{1j} + U_{F,1l} U_{F,3l} U_{S,1m} U_{S,2m} (g_{1i} g_{2j} + g_{1j} g_{2i}) + U_{F,1l}^2 (U_{S,2m}^2 - U_{S,3m}^2) g_{2i} g_{2j} \right], \quad (4.1)$$

which can be written as $M_\nu = g^T M g$ with the scalar-fermion coupling matrix

$$g = \begin{pmatrix} g_{11} & g_{12} & g_{13} \\ g_{21} & g_{22} & g_{23} \end{pmatrix}, \quad (4.2)$$

the elements of the symmetric matrix M

$$\begin{aligned} M_{11} &= \sum_{l,m} m_{lm} U_{F,3l}^3 U_{S,1m}^2, \\ M_{12} &= \sum_{l,m} m_{lm} U_{F,1l} U_{F,3l} U_{S,1m} U_{S,2m} = M_{21}, \\ M_{22} &= \sum_{l,m} m_{lm} U_{F,1l}^2 (U_{S,2m}^2 - U_{S,3m}^2) \end{aligned} \quad (4.3)$$

and the mass function

$$m_{lm} = \frac{1}{16\pi^2} \frac{M_{\chi_l}}{M_{X_m}^2 - M_{\chi_l}^2} \left(M_{\chi_l}^2 \ln M_{\chi_l}^2 - M_{X_m}^2 \ln M_{X_m}^2 \right). \quad (4.4)$$

In the limit of vanishing λ_S , λ_D etc. and small values of $A, y_1, y_2 \ll 1$, the matrix elements of M can be expanded and expressed as

$$\begin{aligned} M_{11} &\propto (A^2 - \text{const.})y^2, \\ M_{12} &\propto Ay, \\ M_{22} &\propto A^2. \end{aligned} \tag{4.5}$$

This demonstrates that the generation of non-zero neutrino masses requires non-vanishing values of g_{ij} , A , y_1 and/or y_2 . In the opposite limit of vanishing A , y_1 , y_2 etc. and small values of λ_D'' , one finds

$$\begin{aligned} M_{11} &= 0, \\ M_{12} &= 0, \\ M_{22} &\propto \lambda_D'', \end{aligned} \tag{4.6}$$

i.e. the neutrino masses are proportional to the doublet scalar mass splitting.

The diagonalization of the neutrino mass matrix $D_\nu = U_\nu^T M_\nu U_\nu = (0, m_{\nu_2}, m_{\nu_3})$ with the PMNS matrix U_ν leads to two non-zero Majorana neutrino masses, while the third mass is always zero. The observed neutrino mass differences [43] then translate directly to absolute neutrino masses. A third non-zero neutrino mass could in principle be accommodated, but would require at least an additional scalar or fermion singlet. Assuming normal mass hierarchy, the experimental constraints on the neutrino masses and mixing angles translate directly into constraints on the couplings [44]

$$g = U_M D_M^{-\frac{1}{2}} R D_\nu^{\frac{1}{2}} U_\nu^T, \tag{4.7}$$

where U_M diagonalises M via $D_M = U_M^T M U_M$ and the rotation matrix

$$R = \begin{pmatrix} 0 & \cos \varphi & -\sin \varphi \\ 0 & \sin \varphi & \cos \varphi \end{pmatrix} \tag{4.8}$$

depends on a single parameter φ . For definiteness, we take all parameters entering Eq. (4.7) to be real, *i.e.* the Dirac and Majorana phases in U_ν and the phase associated with R are assumed to be zero.

From Eq. (4.1) it is clear that in the absence of all scalar-fermion couplings g_{ij} , neutrino masses cannot be generated. The neutrino masses depend, however, also on the dark mass spectrum and, through the fermion and scalar mixing matrices U_F and U_S , on the Yukawa couplings y_1 and y_2 , the singlet-doublet scalar coupling A and, to a lesser extent, on the exclusively singlet or doublet scalar couplings λ_S , λ_D etc. This can also be seen from Fig. 2 of Ref. [19] before electroweak symmetry breaking, which involves all four dark mass parameters as well as the couplings g_{ij}^2 , y_1 or y_2 , and A , but not λ_S , λ_D etc. In the following numerical studies of the total neutrino mass sum, we therefore fix the latter to values of $\mathcal{O}(10^{-1})$ or smaller.

In Fig. 7, we demonstrate the influence of the scalar-fermion couplings g_{ij} on the sum

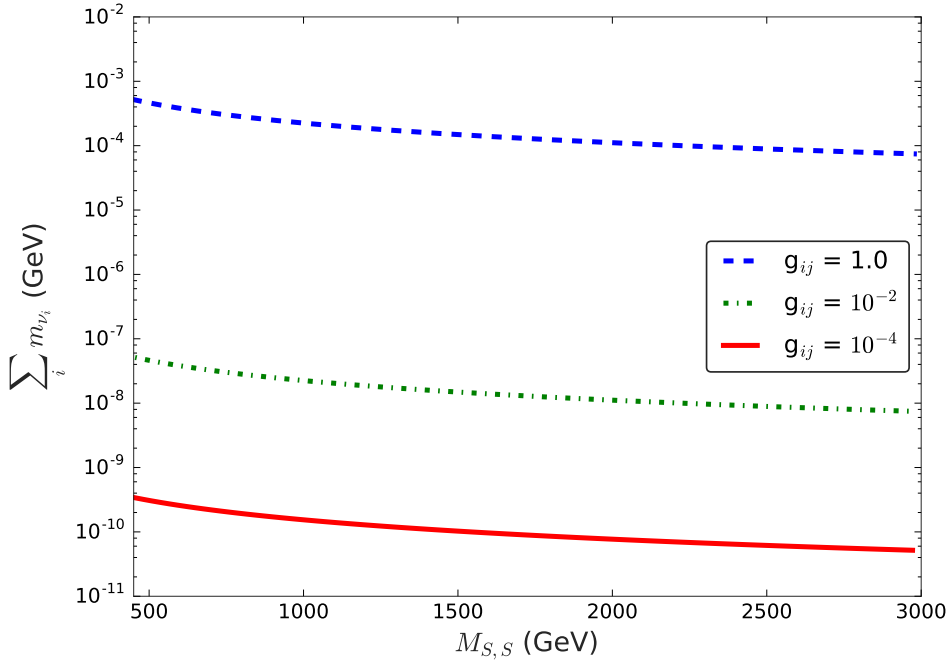


Figure 7. Influence of the scalar-fermion couplings g_{ij} on the sum of neutrino masses as a function of the singlet scalar mass parameter $M_{S,S}$.

of neutrino masses as a function of the scalar singlet mass $M_{S,S}$. The other masses are scaled to it via $M_{D,S} = 1.5 M_{S,S}$, $M_{S,F} = 2 M_{S,S}$ and $M_{D,F} = 2.5 M_{S,S}$, and the scalar and Yukawa couplings are small ($A = 10^{-2}$ GeV, $y_1 = 2 \cdot 10^{-2}$, and $y_2 = 10^{-1}$). Therefore, the singlet scalar and doublet fermion dominate, at least to some extent, in the loop. As the singlet scalar mass (and with it all other masses) increases, the neutrino masses decrease moderately as expected from the propagator suppression in the loop. More importantly, as the scalar-fermion couplings g_{ij} , and in particular the singlet scalar-doublet fermion couplings g_{1i} , decrease from values of 1 (dashed blue line) to 10^{-2} (dot-dashed green line) and 10^{-4} (full red line), the neutrino mass sum drops over eight orders of magnitude in agreement with the quadratic scaling of $M_{\nu,ij}$ with g_{ij} in Eq. (4.1). In this scenario, the viable region of $\sum_i m_{\nu_i} = \mathcal{O}(10^{-11})$ GeV is thus reached only for very small values of g_{ij} .

This is, however, not always the case, as we demonstrate in Fig. 8. Here, the neutrino mass sum is shown as a function of the singlet fermion mass $M_{S,F}$, while the other masses are scaled to it via $M_{S,S} = 2.5 M_{S,F}$, $M_{D,S} = 3.5 M_{S,F}$ and $M_{D,F} = 1.5 M_{S,F}$. The doublet scalar mass is substantially larger than in the previous figure, and it mixes strongly ($A = 10$ GeV) with the singlet scalar, while the Yukawa couplings are comparable ($y_1 = 4 \cdot 10^{-2}$, $y_2 = 2 \cdot 10^{-2}$), so that the dominance of the singlet fermion and the doublet scalar in the loop is less pronounced. In total, this leads to neutrino mass sums that are at least an order of magnitude smaller and fall more steeply for small $M_{S,F}$. The striking feature in Fig. 8 is the cancellation of terms of opposite sign in Eq. (4.1) that leads to a vanishingly

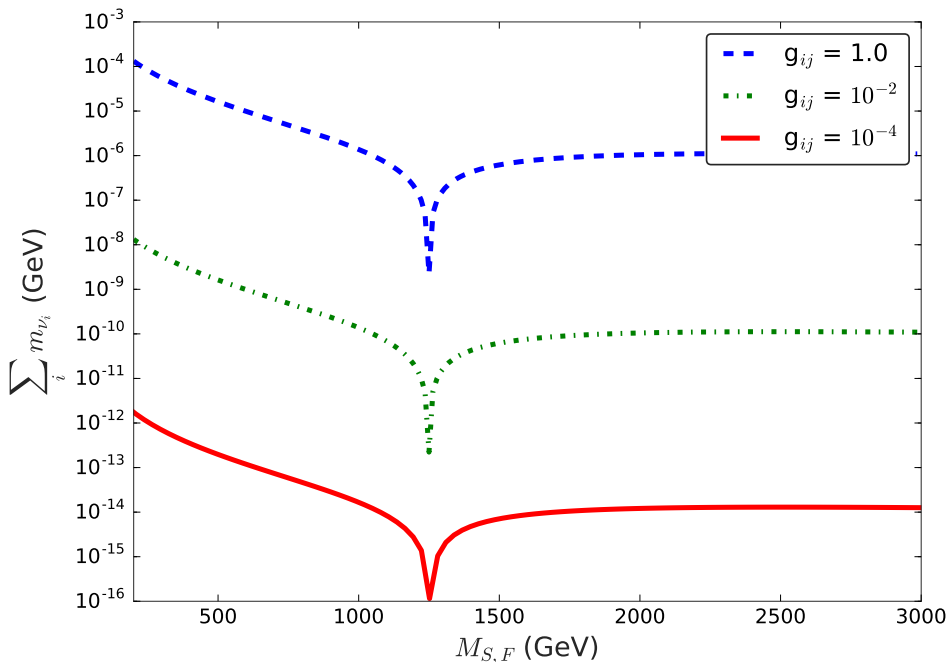


Figure 8. Influence of the scalar-fermion couplings g_{ij} on the sum of neutrino masses as a function of the singlet fermion mass parameter $M_{S,F}$.

small neutrino mass sum around $M_{S,F} = 1.25$ TeV. Outside this region, one observes the same quadratic scaling with g_{ij} from 1 (dashed blue line) over 10^{-2} (dot-dashed green line) to 10^{-4} (full red line) as before, but due to the larger masses and cancellations, the viable neutrino mass region can now already be reached for intermediate values of g_{ij} .

In Fig. 9, we investigate the influence of the Yukawa couplings y_1 and y_2 on the sum of neutrino masses for singlet scalar dark matter of mass $M_{S,S} = 1$ TeV, which does not mix with the doublet scalar ($A = 0$), but couples to the doublet fermion with fixed strength $g_{1i} = 0.1$. The other couplings λ_S , λ_D etc. and g_{2i} have no significant impact and have been set to values of 10^{-5} . The doublet scalar and singlet fermion have thus also no obvious direct influence, and their masses have been decoupled with fixed mass ratios of $M_{S,S}/M_{D,S} = 0.3$ and $M_{S,S}/M_{S,F} = 0.6$, respectively. For large doublet fermion masses (top left), one observes that the full range of Yukawa couplings shown leads to a sum of neutrino masses of $\mathcal{O}(10^{-11})$ GeV or smaller. If both Yukawa couplings y_1 and y_2 are of similar size, they can be larger than when this is true for only one of them. As the doublet fermion mass decreases and approaches the scalar singlet mass (bottom right), the Yukawa couplings also drop in order for the neutrino masses to remain in the viable observed range. Interestingly, they can not be too small either once the doublet fermion mass drops below the singlet fermion mass (beyond $M_{S,S}/M_{S,F} = 0.3$). The doublet fermion then has to mix more with the singlet fermion to reduce the neutrino mass to the viable region.

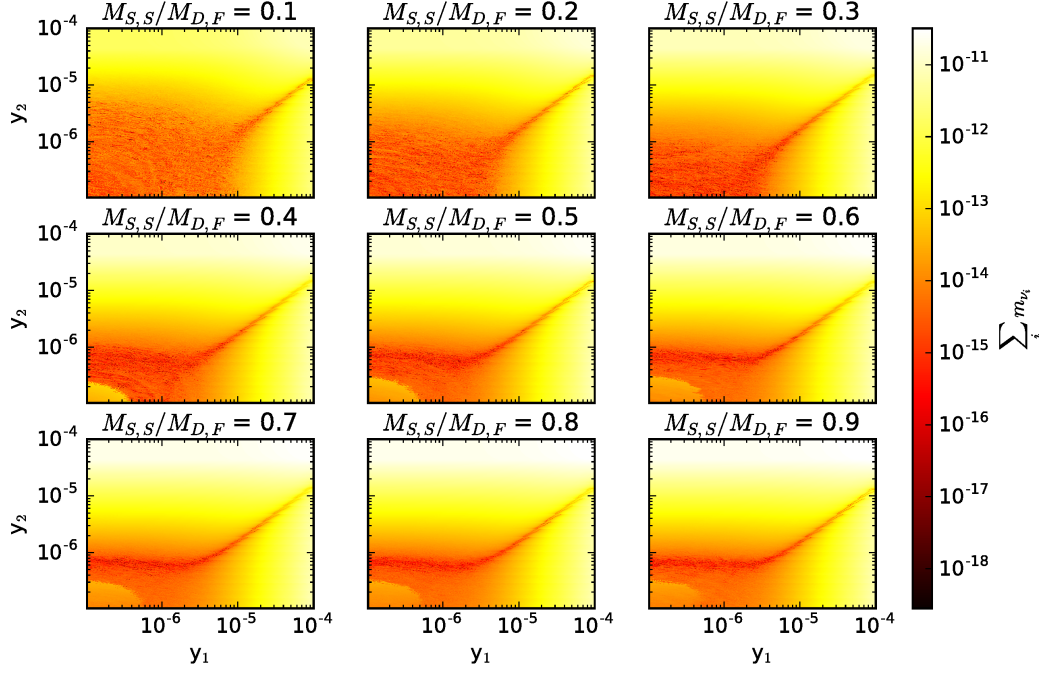


Figure 9. Influence on the ratio of the singlet scalar mass $M_{S,S} = 1$ TeV over the singlet fermion mass $M_{S,F}$ on the sum of neutrino masses in the plane of Yukawa couplings y_1 - y_2 . The doublet scalar and singlet fermion have been decoupled via $M_{S,S}/M_{D,S} = 0.6$ and $M_{S,S}/M_{S,F} = 0.3$.

5 Lepton flavour violation

The radiative generation of neutrino masses in our model implies the existence of lepton-number violating terms in the Lagrangian and thus of lepton-flavour violating processes. Important examples are the radiative transitions $\mu \rightarrow e\gamma$ etc., the leptonic decays $\mu \rightarrow 3e$ etc., and conversion processes such as $\mu \text{Au} \rightarrow e \text{Au}$. The first class of transitions arises through the bubble (top) or triangle (bottom) diagrams depicted in Fig. 10, where always both new scalars and fermions must run in the loops. Neglecting the external lepton masses, the branching ratio can be expressed as

$$\text{BR}(\mu \rightarrow e\gamma) = \frac{3\alpha_{em}}{64\pi G_F^2} \left[\frac{1}{2m_{\psi^-}^4} \left(\sum_i g_{11}g_{12}U_{S,1i}^2 F\left(\frac{m_{X_i}^2}{m_{\psi^-}^2}\right) \right)^2 + \frac{1}{m_{\phi^-}^4} \left(\sum_i g_{21}g_{22}U_{F,1i}^2 F\left(\frac{m_{X_i}^2}{m_{\phi^-}^2}\right) \right)^2 + \frac{1}{m_{\phi^-}^2 m_{\psi^-}^2} \left(\sum_i g_{11}g_{12}U_{S,1i}^2 F\left(\frac{m_{X_i}^2}{m_{\psi^-}^2}\right) \right) \left(\sum_j g_{21}g_{22}U_{F,1j}^2 F\left(\frac{m_{X_j}^2}{m_{\phi^-}^2}\right) \right) \right] \quad (5.1)$$

with

$$F(x) = \frac{2x^3 + 3x^2 - 6x^2 \ln x - 6x + 1}{6(x-1)^4} \quad (5.2)$$

and similarly for $\tau \rightarrow e\gamma$ and $\tau \rightarrow \mu\gamma$. It is obvious that in the limit of vanishing scalar-fermion couplings $g_{ij} \rightarrow 0$, not only the neutrino masses, but also the lepton-flavour violat-

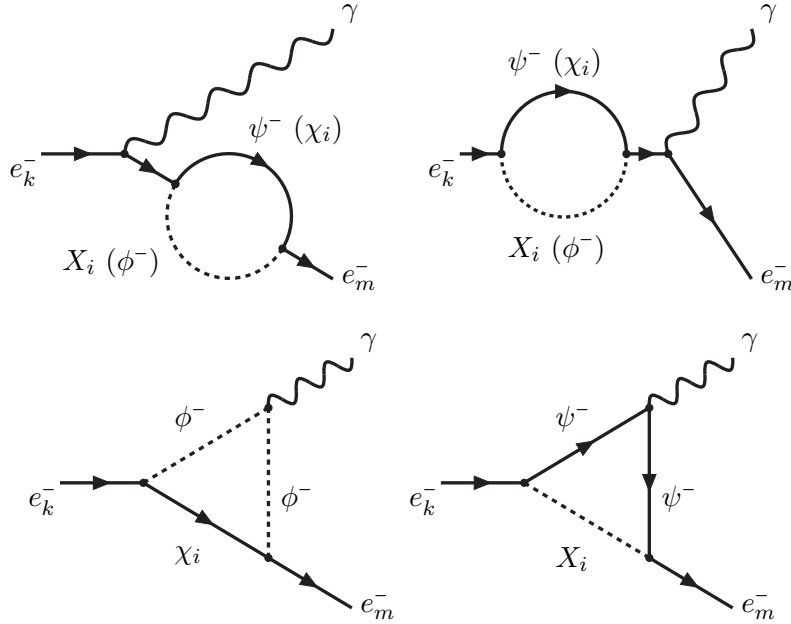


Figure 10. Radiative one-loop processes $e_k^- \rightarrow e_m^- \gamma$ violating lepton flavour.

ing processes disappear. While the neutrino mass matrix in Eq. (4.1) always depends on both the dark scalar and fermion mixing matrices U_S and U_F , the charged lepton processes always require one charged dark particle in the loop, so that they depend at the amplitude level only on one of the neutral mixing matrices. The same diagrams as in Fig. 10 also contribute to conversion processes, when the photon is taken off-shell and couples to the heavy nucleus. The flavour-violating leptonic decay processes $\mu \rightarrow 3e$ etc. are mediated by the diagrams shown in Fig. 11. They involve bubble, triangle and box one-loop topologies and thus at the amplitude level two (bubbles and triangles) or four (boxes) powers of scalar-fermion couplings g_{ij} and mixing matrices.

Current and future limits on the branching ratios for the processes described above are listed in Tab. 2. As one can see, the process $\mu \rightarrow e\gamma$ typically sets the most stringent limits on new particle masses and couplings. We therefore show in Fig. 12 the dependence of the branching ratio for this process on the singlet scalar mass $M_{S,S}$. All other parameters have been set as in Fig. 7 to allow for an easy comparison with the corresponding neutrino masses. In particular, we show again three curves for scalar-fermion couplings g_{ij} of 1 (dashed blue curve), 10^{-2} (dot-dashed green curve) and 10^{-4} (full red curve). As expected, the branching ratio falls with the singlet scalar mass in the loop, but much more directly with the scalar-fermion couplings g_{ij} . Current and future experimental limits can be evaded already with values of 10^{-2} , whereas the neutrino masses required even smaller values of about 10^{-4} for these couplings.

6 Numerical results

In this section, we present our main numerical results. We focus on the case of scalar dark matter and perform two random numerical scans, the first over the full parameter

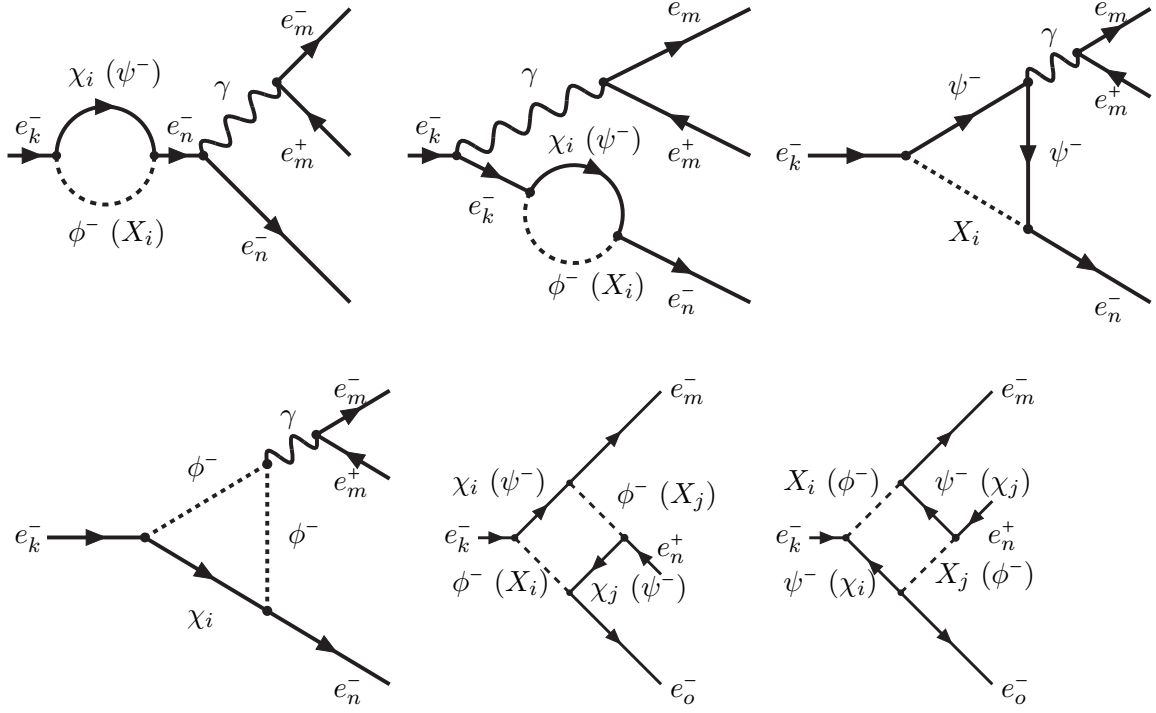


Figure 11. Loop diagrams contributing to the leptonic decays $e_k^- \rightarrow e_m^- e_n^+ e_o^-$

Table 2. Current and future limits on lepton-flavour violating processes.

Process	Current limit	Future expectation
$\mu \rightarrow e\gamma$	5.7×10^{-13} [45]	6×10^{-14} [46]
$\tau \rightarrow e\gamma$	3.3×10^{-8} [47]	$\approx 3 \times 10^{-9}$ [48]
$\tau \rightarrow \mu\gamma$	4.4×10^{-8} [47]	$\approx 3 \times 10^{-9}$ [48]
$\mu \rightarrow 3e$	1.0×10^{-12} [49]	$\approx 10^{-16}$ [50]
$\tau \rightarrow 3\mu$	2.1×10^{-8} [51]	$\approx 10^{-9}$ [48]
$\tau^- \rightarrow e^- \mu^+ \mu^-$	2.7×10^{-8} [51]	$\approx 10^{-9}$ [48]
$\tau^- \rightarrow \mu^- e^+ e^-$	1.8×10^{-8} [51]	$\approx 10^{-9}$ [48]
$\tau \rightarrow 3e$	2.7×10^{-8} [51]	$\approx 10^{-9}$ [48]
$\mu^- \text{Ti} \rightarrow e^- \text{Ti}$	4.3×10^{-12} [52]	$\approx 10^{-18}$ [53]
$\mu^- \text{Au} \rightarrow e^- \text{Au}$	7.0×10^{-13} [54]	–
$\mu^- \text{Al} \rightarrow e^- \text{Al}$	–	$10^{-15} - 10^{-18}$ [55]
$\mu^- \text{SiC} \rightarrow e^- \text{SiC}$	–	10^{-14} [56]

space, the second in a region where coannihilation processes of singlet scalar and doublet fermion processes become important. We impose all available experimental constraints, in particular on the mass $M_H = 125$ GeV and SM couplings of the Higgs boson [43], the observed dark matter relic density $\Omega^{\text{obs}} h^2 = 0.1186 \pm 0.0031$ [12], and the neutrino masses and mixing angles [5]. Limits on the direct detection cross section and lepton-flavour violating processes (cf. Tab. 2) are shown explicitly for the first scan and imposed on the second scan. In both cases, we have obtained $\mathcal{O}(10^4)$ viable points. Possible LHC

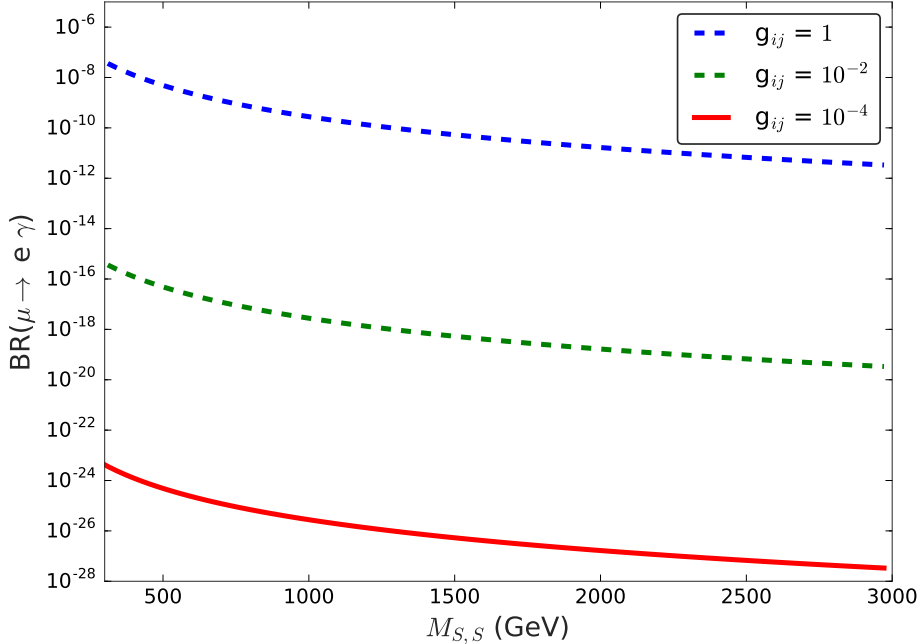


Figure 12. Influence of the scalar-fermion couplings g_{ij} on the branching ratio $\text{BR}(\mu \rightarrow e\gamma)$ as a function of the singlet scalar mass parameter $M_{S,S}$.

constraints are discussed at the end of this section.

6.1 Random scan

In our first random scan, we vary all new masses from 200 GeV to 2 TeV, the scalar couplings in the range $|\lambda_S|, |\lambda_D|, |\lambda'_D|, \lambda''_D \in [0; 2\pi]$, the singlet-doublet scalar coupling $A \in [0; 10^4]$ GeV, the Yukawa couplings $|y_1|, y_2 \in [0; 1]$, and the scalar-fermion couplings are either zero or varied in the range $|g_{ij}| \in [0; 2\pi]$. They are then constrained directly by the neutrino masses and mixing angles through the parameterisation in Eq. (4.7).

In Fig. 13, we plot the spin-independent direct detection cross section σ_{SI} as a function of the physical mass of scalar dark matter, which can be a mixture of the singlet and doublet. In particular, their mixing can be large and lead to physical masses of a few GeV despite the fact that the scanned mass parameters lie above 200 GeV. When the scalar dark matter does not couple to fermions (blue crosses), it is well known that the narrow relic density constraint is strongly correlated with the direct detection cross section. This leads to a narrow band below and on the Higgs resonance at $M_{\text{DM}} \simeq M_H/2$, which becomes somewhat wider above. For constant Ωh^2 , the Higgs coupling and direct detection cross section get smaller as the DM mass increases towards the Higgs resonance. On the resonance, annihilation is very efficient and the couplings and direct detection cross section must be very small. As expected for singlet-doublet scalar dark matter alone [32, 33], most of the parameter points are now excluded by PandaX [57, 58] (dashed curve) and

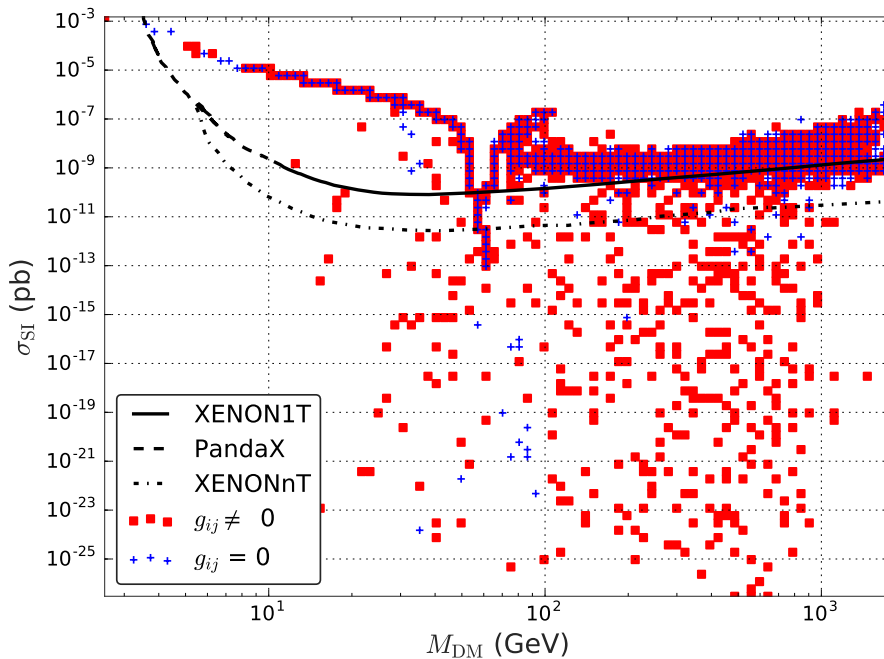


Figure 13. Direct detection cross section of scalar singlet dark matter as a function of its mass without (blue) and with (red) coupling of the scalar to the fermion sector.

XENON1T [59] (full curve). Furthermore, they obviously cannot explain the neutrino masses. The coupling to the fermion sector opens up new regions of parameter space (red squares) allowed by all experimental constraints that cannot even be probed by XENONnT [60], since the direct detection cross section is independent of the couplings g_{ij} . The correct relic density is reached through annihilation processes into leptons and/or scalar-fermion coannihilations.

As Fig. 14 shows, most of the new points are, however, excluded by the lepton-flavour branching ratio $\text{BR}(\mu \rightarrow e\gamma)$. Nevertheless, some of them fulfill in fact all current experimental constraints. Interestingly, they lead to direct detection cross sections that will soon be tested by XENONnT.

6.2 Coannihilation region

In our second scan, we focus on scalar dark matter of mass $M_{S,S} \in [10; 3000]$ GeV, which can coannihilate with doublet fermions of mass $M_{D,F} = [1.05; 1.2] M_{S,S}$, so that these processes contribute at least 50% to the relic density cross section. Doublet scalars and singlet fermions have larger masses of $[1.5 M_{S,S}; 3 \text{ TeV}]$ and $[M_{D,F}; 3 \text{ TeV}]$, respectively. We limit the mixing in the scalar and fermion sectors by reducing the scan ranges of $|\lambda_S|$, A , $|y_1|$ and y_2 to values below $\pi \cdot 10^{-4}$. This also enhances the annihilation into lepton final states.

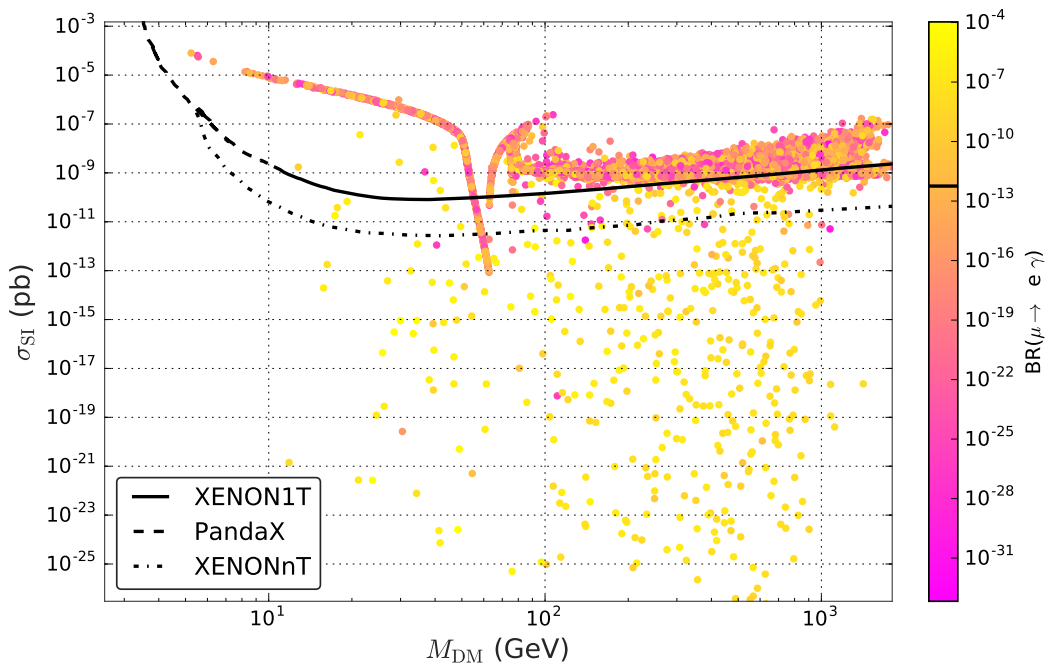


Figure 14. Direct detection cross section of scalar singlet dark matter as a function of its mass and its correlation with the lepton-flavour violating branching ratio $BR(\mu \rightarrow e\gamma)$ (colours).

After imposing all experimental constraints, including those on the direct detection cross section and lepton-flavour violating processes, we obtain the scalar-fermion couplings g_{ij} shown in Fig. 15. Since A , y_1 and y_2 are now all small, we can obtain viable neutrino masses for sizeable values of g_{ij} . As Fig. 15 shows, at least one of these couplings must be large, but they cannot be both large at the same time, which reflects the two rather different neutrino mass differences. Due to the weaker limits on lepton-flavour violation for processes involving the τ lepton, the values of g_{13} are less restricted than those of g_{11} and g_{12} . As the singlet scalar mass $M_{S,S}$ and with it the doublet fermion mass $M_{D,F}$ increase, so must the couplings g_{ij} to compensate for the propagator suppression in the neutrino mass loops. Conversely, as λ_D'' and with it the doublet scalar mass splitting and the neutrino masses increase (cf. Eq. 4.6), the corresponding scalar-fermion couplings g_{2i} must decrease for the neutrino masses to remain in the viable range.

A similar plot to the one in Fig. 15 for g_{1i} shows the plane of the Yukawa couplings $|y_1|$ - y_2 in Fig. 16. Again, one of these couplings, but not both must be relatively large, in particular when the singlet fermion is decoupled (blue points). However, when it becomes light (green points), mixes with the doublet fermion and contributes to coannihilation, smaller values for both Yukawa couplings also become viable.

The direct detection cross section is governed by the coupling λ_S of the scalar singlet to the Higgs boson. It ranges from 10^{-27} pb for $\lambda_S = 10^{-9}$ to 10^{-14} pb for $\lambda_S = 10^{-4}$ and is thus beyond the reach even of XENONnT. The situation is therefore similar to the one in

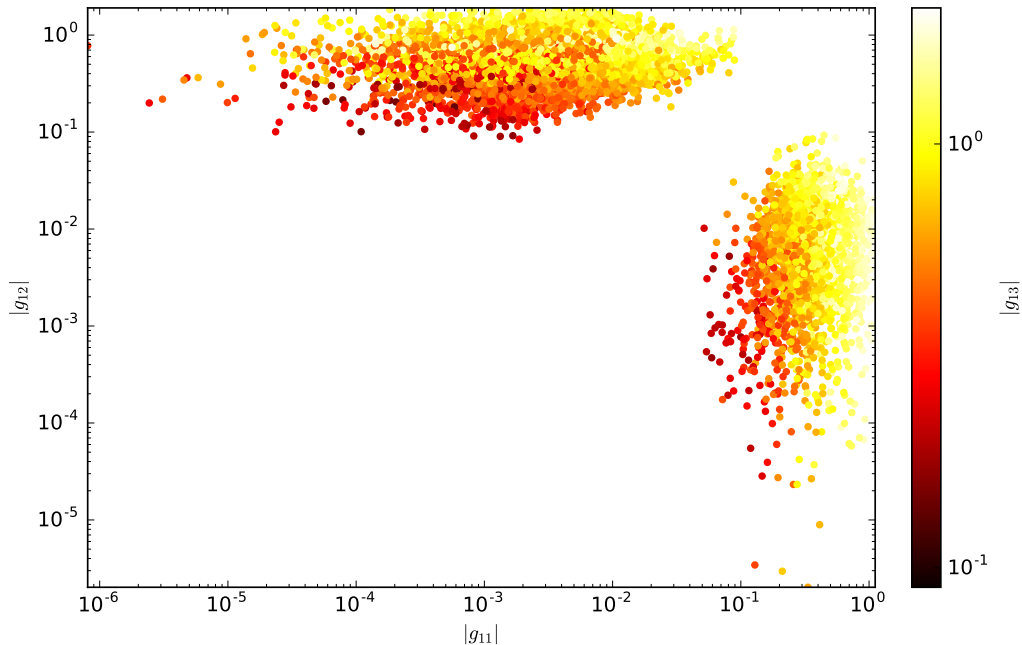


Figure 15. Viable scalar-fermion couplings in the plane $|g_{11}|-|g_{12}|$ (colour code for $|g_{13}|$).

the previous section, where many new viable models had very small direct detection cross sections and had to be constrained by lepton-flavour violating processes. We therefore present in Fig. 17 the branching ratios $\text{BR}(\mu \rightarrow e\gamma)$, $\text{BR}(\tau \rightarrow e\gamma)$ and $\text{BR}(\mu \rightarrow 3e)$. Current and future experimental limits are indicated by full and dashed black lines. Since we impose the current limits on our scan, no excluded models are found. A substantial fraction of the viable models will be tested by future muon decay experiments in either of the two channels, while the sensitivity of future tau decay experiments remains limited and would have to be improved by at least two orders of magnitude to completely probe the upper one of the two viable parameter regions, where g_{11} stays relatively constant.

6.3 LHC constraints

In our first random scan over the full parameter space of scalar dark matter, the latter can be a mixture of singlet and doublet. Various collider limits on either case, in particular from Higgs invisible decays at the LHC and the charged scalar partners at LEP and the LHC, have been discussed in the past [61].

If dark matter is dominated by the singlet component, as it is also the case in our second random scan over the scalar-fermion coannihilation region, it couples neither to the photon nor to the weak gauge bosons, but only to the Higgs boson through the coupling λ_S . Constraints from the LHC thus currently come only from the invisible decay width of the Higgs boson in a mass region below 62.5 GeV. The upper limits lie currently at

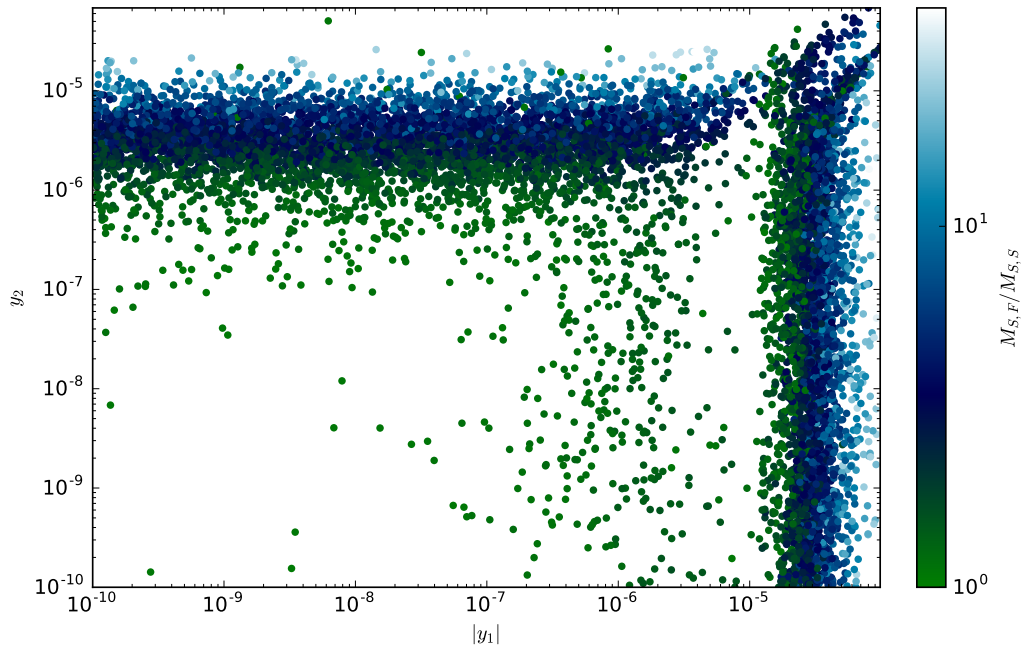


Figure 16. Viable Yukawa couplings in the plane $|y_1|$ - $|y_2|$ (colour code for the mass ratio $M_{S,F}/M_{S,S}$).

67% for associated ZH production in ATLAS [62] and 24% for a combination of different production channels in CMS [63]. As our Fig. 14 and Fig. 8b in Ref. [63] show, models with such large couplings are already ruled out by direct detection and/or $\text{BR}(\mu \rightarrow e\gamma)$.

If the scalar dark matter is dominated by the doublet component, it couples also to the weak gauge bosons. LHC constraints then come in addition from events with a single jet [64] and/or vector boson [65] and large transverse momentum imbalance. They have only been interpreted for fermion dark matter as a function of the mediator mass. If we take the spin to be of minor importance and the mediator to be Z -like in coupling and mass, the limits on the dark matter mass in Figs. 5 and 6 of Ref. [64] and Fig. 10 of Ref. [65] lie at 50–100 GeV, so that the LHC would exclude only a few models beyond the Higgs resonance region. These limits apply more directly to the case of fermion dark matter, which we have not discussed.

Alternatively, heavier charged and/or neutral scalars can be produced at the LHC through weak gauge bosons. They decay subsequently into dark matter and W - or Z -bosons, leading to two- or multi-lepton signals with missing transverse energy (see Fig. 18 left) [66]. These signals have been analysed at the LHC mostly in the context of charged scalar leptons appearing in supersymmetric models. Scalar neutrinos are so far unconstrained by the LHC. Although the charged sleptons do not translate directly into our model, since they decay into fermionic neutralino dark matter in supersymmetry, we can again assume spin to be of minor importance and our charged scalars to decay into

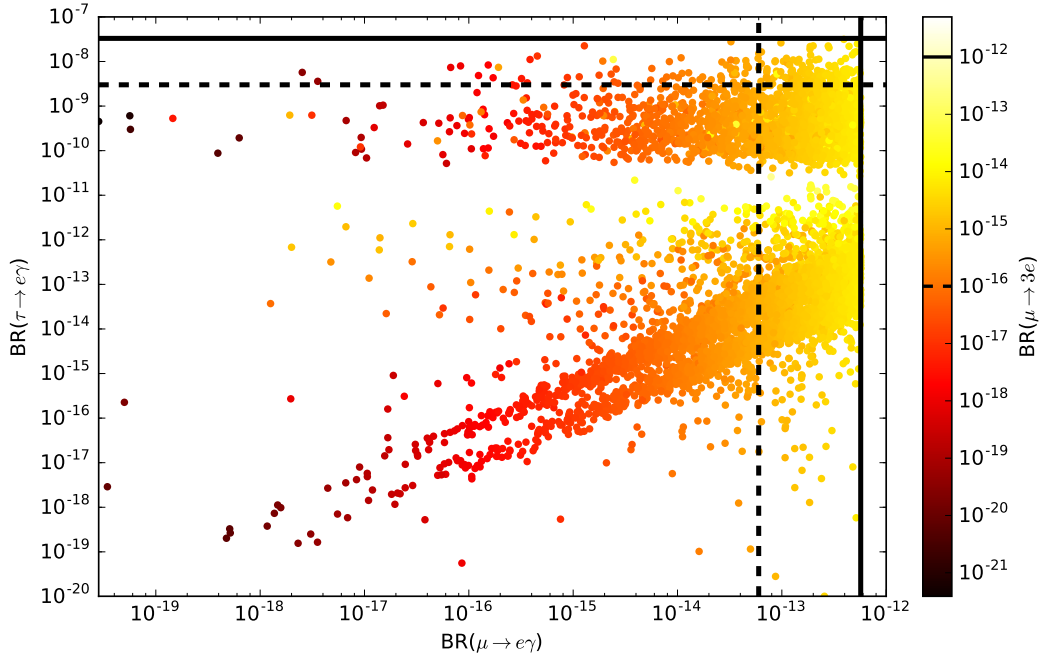


Figure 17. Predicted branching ratios for the most sensitive lepton-flavour violating processes $\text{BR}(\mu \rightarrow e\gamma)$, $\text{BR}(\tau \rightarrow e\gamma)$ and $\text{BR}(\mu \rightarrow 3e)$ (colour) with current (full black lines) and future (dashed black lines) exclusion limits.

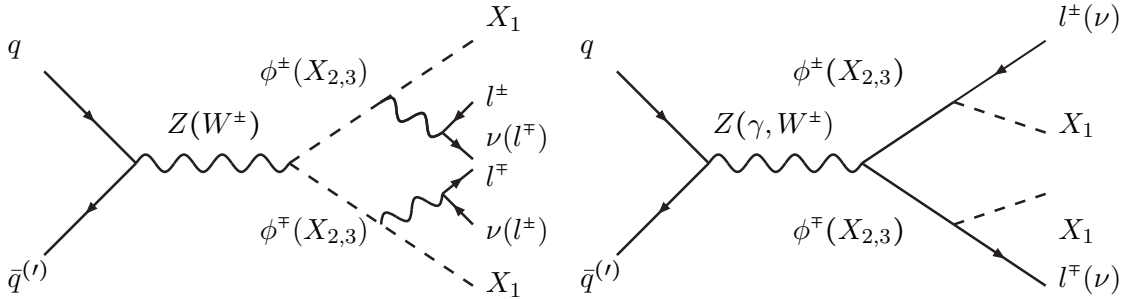


Figure 18. Typical diagrams for the production of heavy scalars (left) and fermions (right) decaying into two- or multi-lepton final states and missing transverse energy, carried away by scalar dark matter X_1 and neutrinos.

the lightest neutral scalars and weak bosons with branching ratios of one, which leads to the strongest constraints. Similar assumptions are also used in the slepton analyses of ATLAS [67] and CMS [68], which leads to lower slepton mass limits of 520 GeV in Fig. 6b of Ref. [67] and 440 GeV in Fig. 3 of Ref. [68]. The corresponding mass limits for dark matter then range from 50-280 GeV and 40-220 GeV, respectively, which would in principle exclude some of the models beyond the Higgs resonance region in Fig. 14. The limits in our model will, however, be considerable weaker since one has to take into account in addition

the leptonic branching fractions of the W - and Z -bosons of 21% and 7% for electrons and muons, respectively. If the charged scalars are heavier than 440-520 GeV or if they have other (e.g. cascade) decays, the LHC limits of course no longer apply at all.

Doublet fermions, which coannihilate in our second random scan with singlet dark matter, can be constrained in a similar way, in particular from searches for higgsino-like charginos and neutralinos (see Fig. 18 right) [26]. Their masses have been constrained by LEP and ATLAS in Fig. 10 of Ref. [69] to be at least 95-145 GeV and by CMS in Fig. 8 of Ref. [70] to be at least 100-170 GeV. The fermionic neutralino dark matter mass then has to be 95-140 GeV and 100-150 GeV, respectively. This would not affect many of our viable models in Fig. 14 beyond the Higgs resonance region. However, the limits in our model will here be stronger, since one does not have into account the leptonic branching fractions of the W and Z -bosons. For singlet-doublet fermion dark matter with scalar singlets, the charged fermions have been shown to require masses of at least 510 GeV [26].

7 Conclusion

In conclusion, we have analysed in this paper a combination of the singlet-doublet scalar and singlet-doublet fermion dark matter models, which had so far only been analysed separately. Their combination allowed for the radiative generation of neutrino masses, but also admitted lepton-flavour violating processes.

After discussing the analytic structure and main parameter dependencies of the model and the implications for the dark matter relic density, neutrino masses and lepton flavour violation, we performed two random scans of the parameter space, focusing on the case of scalar dark matter.

In the first scan over the full parameter space, we imposed constraints from the Higgs mass, relic density and neutrino masses and mixings using the Casas-Ibarra parameterisation. We found that the scalar dark matter could be a mixture of singlets and doublets and in particular that the scalar-fermion couplings opened up large new regions of parameter space, mostly with direct detection cross sections that will escape experimental verification way beyond XENONnT. Many of these models were instead shown to be excluded by lepton-flavour violation constraints. The remaining viable models will soon be probed by XENONnT.

In the second scan, we focused on singlet scalar dark matter coannihilating with mostly doublet fermions. In this case we also imposed constraints from direct detection and lepton-flavour violation experiments. We found that at least one of the scalar-fermion couplings and Yukawa couplings had to be large or not too small, respectively, leading to two distinct regions in parameter space. Many of these models will soon be tested by experiments on $\mu \rightarrow e\gamma$ or $\mu \rightarrow 3e$, while those on $\tau \rightarrow e\gamma$ would require an increase of at least two more orders of magnitude beyond current planning to allow for the complete testing of at least one of the two viable regions in parameter space.

LHC constraints from invisible Higgs decays were shown to add no further constraints on the models with dark matter masses below the Higgs resonance, while monojet, mono-boson and in particular dilepton searches have in principle the potential to reach into the

region beyond it up to 280 GeV. These limits depend, however, crucially on the heavier and in particular charged particle mass spectrum and decay modes. A full analysis of the model would require detailed information on acceptances and efficiencies of the LHC experiments and is beyond the scope of this work.

Acknowledgments

We thank K. Kovarik, S. May and M. Sunder for useful discussions. This work has been supported by the DFG through the Research Training Network 2149 “Strong and weak interactions - from hadrons to dark matter”.

References

- [1] **ATLAS** Collaboration, G. Aad *et. al.*, *Observation of a new particle in the search for the Standard Model Higgs boson with the ATLAS detector at the LHC*, *Phys. Lett.* **B716** (2012) 1–29, [[1207.7214](#)].
- [2] **CMS** Collaboration, S. Chatrchyan *et. al.*, *Observation of a new boson at a mass of 125 GeV with the CMS experiment at the LHC*, *Phys. Lett.* **B716** (2012) 30–61, [[1207.7235](#)].
- [3] H. Georgi, H. R. Quinn, and S. Weinberg, *Hierarchy of Interactions in Unified Gauge Theories*, *Phys. Rev. Lett.* **33** (1974) 451–454.
- [4] M. J. G. Veltman, *The Infrared - Ultraviolet Connection*, *Acta Phys. Polon.* **B12** (1981) 437.
- [5] M. C. Gonzalez-Garcia, M. Maltoni, and T. Schwetz, *Updated fit to three neutrino mixing: status of leptonic CP violation*, *JHEP* **11** (2014) 052, [[1409.5439](#)].
- [6] **Super-Kamiokande** Collaboration, Y. Fukuda *et. al.*, *Evidence for oscillation of atmospheric neutrinos*, *Phys. Rev. Lett.* **81** (1998) 1562–1567, [[hep-ex/9807003](#)].
- [7] **SNO** Collaboration, Q. R. Ahmad *et. al.*, *Measurement of the rate of $\nu_e + d \rightarrow p + p + e^-$ interactions produced by 8B solar neutrinos at the Sudbury Neutrino Observatory*, *Phys. Rev. Lett.* **87** (2001) 071301, [[nucl-ex/0106015](#)].
- [8] **SNO** Collaboration, Q. R. Ahmad *et. al.*, *Direct evidence for neutrino flavor transformation from neutral current interactions in the Sudbury Neutrino Observatory*, *Phys. Rev. Lett.* **89** (2002) 011301, [[nucl-ex/0204008](#)].
- [9] **KamLAND** Collaboration, T. Araki *et. al.*, *Measurement of neutrino oscillation with KamLAND: Evidence of spectral distortion*, *Phys. Rev. Lett.* **94** (2005) 081801, [[hep-ex/0406035](#)].
- [10] M. Klasen, M. Pohl, and G. Sigl, *Indirect and direct search for dark matter*, *Prog. Part. Nucl. Phys.* **85** (2015) 1–32, [[1507.03800](#)].
- [11] **WMAP** Collaboration, G. Hinshaw *et. al.*, *Nine-Year Wilkinson Microwave Anisotropy Probe (WMAP) Observations: Cosmological Parameter Results*, *Astrophys. J. Suppl.* **208** (2013) 19, [[1212.5226](#)].
- [12] **Planck** Collaboration, P. A. R. Ade *et. al.*, *Planck 2013 results. XVI. Cosmological parameters*, *Astron. Astrophys.* **571** (2014) A16, [[1303.5076](#)].
- [13] E. Ma, *Verifiable radiative seesaw mechanism of neutrino mass and dark matter*, *Phys. Rev.* **D73** (2006) 077301, [[hep-ph/0601225](#)].

- [14] M. Klasen, C. E. Yaguna, J. D. Ruiz-Alvarez, D. Restrepo, and O. Zapata, *Scalar dark matter and fermion coannihilations in the radiative seesaw model*, *JCAP* **1304** (2013) 044, [[1302.5298](#)].
- [15] E. Ma and D. Suematsu, *Fermion Triplet Dark Matter and Radiative Neutrino Mass*, *Mod. Phys. Lett.* **A24** (2009) 583–589, [[0809.0942](#)].
- [16] Y. Farzan, S. Pascoli, and M. A. Schmidt, *AMEND: A model explaining neutrino masses and dark matter testable at the LHC and MEG*, *JHEP* **10** (2010) 111, [[1005.5323](#)].
- [17] M. Aoki, S. Kanemura, and K. Yagyu, *Doubly-charged scalar bosons from the doublet*, *Phys. Lett.* **B702** (2011) 355–358, [[1105.2075](#)]. [Erratum: *Phys. Lett.*B706,495(2012)].
- [18] S. S. C. Law and K. L. McDonald, *A Class of Inert N-tuplet Models with Radiative Neutrino Mass and Dark Matter*, *JHEP* **09** (2013) 092, [[1305.6467](#)].
- [19] D. Restrepo, O. Zapata, and C. E. Yaguna, *Models with radiative neutrino masses and viable dark matter candidates*, *JHEP* **11** (2013) 011, [[1308.3655](#)].
- [20] F. Bonnet, M. Hirsch, T. Ota, and W. Winter, *Systematic study of the d=5 Weinberg operator at one-loop order*, *JHEP* **07** (2012) 153, [[1204.5862](#)].
- [21] C. Simoes and D. Wegman, *Radiative Two-Loop Neutrino Masses with Dark Matter*, *JHEP* **04** (2017) 148, [[1702.04759](#)].
- [22] D. Aristizabal Sierra, A. Degee, L. Dorame, and M. Hirsch, *Systematic classification of two-loop realizations of the Weinberg operator*, *JHEP* **03** (2015) 040, [[1411.7038](#)].
- [23] Y. Cai, J. Herrero-Garcia, M. A. Schmidt, A. Vicente, and R. R. Volkas, *From the trees to the forest: a review of radiative neutrino mass models*, *Front.in Phys.* **5** (2017) 63, [[1706.08524](#)].
- [24] Y. Farzan, *A Minimal model linking two great mysteries: neutrino mass and dark matter*, *Phys. Rev.* **D80** (2009) 073009, [[0908.3729](#)].
- [25] S. Fraser, E. Ma, and O. Popov, *Scotogenic Inverse Seesaw Model of Neutrino Mass*, *Phys. Lett.* **B737** (2014) 280–282, [[1408.4785](#)].
- [26] D. Restrepo, A. Rivera, M. Sanchez-Pelaez, O. Zapata, and W. Tangarife, *Radiative Neutrino Masses in the Singlet-Doublet Fermion Dark Matter Model with Scalar Singlets*, *Phys. Rev.* **D92** (2015), no. 1 013005, [[1504.07892](#)].
- [27] S. Esch, M. Klasen, D. R. Lamprea, and C. E. Yaguna, *Lepton flavor violation and scalar dark matter in a radiative model of neutrino masses*, *Eur. Phys. J.* **C78** (2018) 88, [[1602.05137](#)].
- [28] Y. Farzan, S. Pascoli, and M. A. Schmidt, *Recipes and Ingredients for Neutrino Mass at Loop Level*, *JHEP* **03** (2013) 107, [[1208.2732](#)].
- [29] R. Longas, D. Portillo, D. Restrepo, and O. Zapata, *The Inert Zee Model*, *JHEP* **03** (2016) 162, [[1511.01873](#)].
- [30] A. Betancur, R. Longas, and O. Zapata, *Doublet-triplet dark matter with neutrino masses*, *Phys. Rev.* **D96** (2017), no. 3 035011, [[1704.01162](#)].
- [31] C. Hagedorn, T. Ohlsson, S. Riad, and M. A. Schmidt, *Unification of Gauge Couplings in Radiative Neutrino Mass Models*, *JHEP* **09** (2016) 111, [[1605.03986](#)].
- [32] T. Cohen, J. Kearney, A. Pierce, and D. Tucker-Smith, *Singlet-Doublet Dark Matter*, *Phys. Rev.* **D85** (2012) 075003, [[1109.2604](#)].

- [33] C. Cheung and D. Sanford, *Simplified Models of Mixed Dark Matter*, *JCAP* **1402** (2014) 011, [[1311.5896](#)].
- [34] A. Dutta Banik and D. Majumdar, *Inert doublet dark matter with an additional scalar singlet and 125 GeV Higgs boson*, *Eur. Phys. J.* **C74** (2014), no. 11 3142, [[1404.5840](#)].
- [35] L. G. Cabral-Rosetti, R. Gaitan, J. H. Montes de Oca, R. Osorio Galicia, and E. A. Garcs, *Scalar dark matter in inert doublet model with scalar singlet*, *J. Phys. Conf. Ser.* **912** (2017), no. 1 012047.
- [36] L. Calibbi, A. Mariotti, and P. Tziveloglou, *Singlet-Doublet Model: Dark matter searches and LHC constraints*, *JHEP* **10** (2015) 116, [[1505.03867](#)].
- [37] S. Banerjee, S. Matsumoto, K. Mukaida, and Y.-L. S. Tsai, *WIMP Dark Matter in a Well-Tempered Regime: A case study on Singlet-Doublets Fermionic WIMP*, *JHEP* **11** (2016) 070, [[1603.07387](#)].
- [38] T. Abe, *Effect of CP violation in the singlet-doublet dark matter model*, *Phys. Lett.* **B771** (2017) 125–130, [[1702.07236](#)].
- [39] G. Belanger, F. Boudjema, A. Pukhov, and A. Semenov, *micrOMEGAs4.1: two dark matter candidates*, *Comput. Phys. Commun.* **192** (2015) 322–329, [[1407.6129](#)].
- [40] A. Semenov, *LanHEP A package for automatic generation of Feynman rules from the Lagrangian. Version 3.2*, *Comput. Phys. Commun.* **201** (2016) 167–170, [[1412.5016](#)].
- [41] F. Staub, *SARAH 4 : A tool for (not only SUSY) model builders*, *Comput. Phys. Commun.* **185** (2014) 1773–1790, [[1309.7223](#)].
- [42] W. Porod and F. Staub, *SPheno 3.1: Extensions including flavour, CP-phases and models beyond the MSSM*, *Comput. Phys. Commun.* **183** (2012) 2458–2469, [[1104.1573](#)].
- [43] **Particle Data Group** Collaboration, C. Patrignani *et. al.*, *Review of Particle Physics*, *Chin. Phys.* **C40** (2016), no. 10 100001.
- [44] J. A. Casas and A. Ibarra, *Oscillating neutrinos and muon $\rightarrow e, \gamma$* , *Nucl. Phys.* **B618** (2001) 171–204, [[hep-ph/0103065](#)].
- [45] **MEG** Collaboration, J. Adam *et. al.*, *New constraint on the existence of the $\mu^+ \rightarrow e^+ \gamma$ decay*, *Phys. Rev. Lett.* **110** (2013) 201801, [[1303.0754](#)].
- [46] A. M. Baldini *et. al.*, *MEG Upgrade Proposal*, [[1301.7225](#)].
- [47] **BaBar** Collaboration, B. Aubert *et. al.*, *Searches for Lepton Flavor Violation in the Decays $\tau_{+-} \rightarrow e_{\pm} \gamma$ and $\tau_{+-} \rightarrow \mu_{\pm} \gamma$* , *Phys. Rev. Lett.* **104** (2010) 021802, [[0908.2381](#)].
- [48] T. Aushev *et. al.*, *Physics at Super B Factory*, [[1002.5012](#)].
- [49] **SINDRUM** Collaboration, U. Bellgardt *et. al.*, *Search for the Decay $\mu^+ \rightarrow e^+ e^+ e^-$* , *Nucl. Phys.* **B299** (1988) 1–6.
- [50] A. Blondel *et. al.*, *Research Proposal for an Experiment to Search for the Decay $\mu \rightarrow eee$* , [[1301.6113](#)].
- [51] **Belle** Collaboration, K. Hayasaka *et. al.*, *Search for $\tau \rightarrow e \gamma$ decay at BELLE*, *Phys. Lett.* **B613** (2005) 20–28, [[hep-ex/0501068](#)].
- [52] **SINDRUM II** Collaboration, C. Dohmen *et. al.*, *Test of lepton flavor conservation in $\mu \rightarrow e$ conversion on titanium*, *Phys. Lett.* **B317** (1993) 631–636.

- [53] A. Sato, *Muon storage ring PRISM-FFAG to improve a sensitivity of mu-e conversion experiment below 10^{-17}* , *PoS NFACT08* (2008) 105.
- [54] **SINDRUM II** Collaboration, W. H. Bertl *et. al.*, *A Search for muon to electron conversion in muonic gold*, *Eur. Phys. J.* **C47** (2006) 337–346.
- [55] R. P. Litchfield, *Muon to electron conversion: The COMET and Mu2e experiments*, in *Interplay between Particle and Astroparticle physics (IPA2014) London, United Kingdom, August 18-22, 2014*, 2014. [1412.1406](#).
- [56] **DeeMe** Collaboration, H. Natori, *DeeMe experiment - An experimental search for a mu-e conversion reaction at J-PARC MLF*, *Nucl. Phys. Proc. Suppl.* **248-250** (2014) 52–57.
- [57] **PandaX** Collaboration, A. Tan *et. al.*, *Dark Matter Search Results from the Commissioning Run of PandaX-II*, *Phys. Rev.* **D93** (2016), no. 12 122009, [[1602.06563](#)].
- [58] J. Liu, X. Chen, and X. Ji, *Current status of direct dark matter detection experiments*, *Nature Phys.* **13** (2017), no. 3 212–216, [[1709.00688](#)].
- [59] **XENON** Collaboration, E. Aprile *et. al.*, *First Dark Matter Search Results from the XENON1T Experiment*, *Phys. Rev. Lett.* **119** (2017), no. 18 181301, [[1705.06655](#)].
- [60] **XENON** Collaboration, E. Aprile *et. al.*, *Physics reach of the XENON1T dark matter experiment*, *JCAP* **1604** (2016), no. 04 027, [[1512.07501](#)].
- [61] T. Abe, R. Kitano, and R. Sato, *Discrimination of dark matter models in future experiments*, *Phys. Rev.* **D91** (2015), no. 9 095004, [[1411.1335](#)]. [Erratum: *Phys. Rev.* **D96**, no. 1, 019902(2017)].
- [62] **ATLAS** Collaboration, M. Aaboud *et. al.*, *Search for an invisibly decaying Higgs boson or dark matter candidates produced in association with a Z boson in pp collisions at $\sqrt{s} = 13$ TeV with the ATLAS detector*, *Phys. Lett.* **B776** (2018) 318–337, [[1708.09624](#)].
- [63] **CMS** Collaboration, C. Collaboration, *Search for invisible decays of the Higgs boson produced through vector boson fusion at $\sqrt{s} = 13$ TeV*, .
- [64] **ATLAS** Collaboration, M. Aaboud *et. al.*, *Search for dark matter and other new phenomena in events with an energetic jet and large missing transverse momentum using the ATLAS detector*, *JHEP* **01** (2018) 126, [[1711.03301](#)].
- [65] **CMS** Collaboration, A. M. Sirunyan *et. al.*, *Search for new physics in final states with an energetic jet or a hadronically decaying W or Z boson and transverse momentum imbalance at $\sqrt{s} = 13$ TeV*, [1712.02345](#).
- [66] E. Dolle, X. Miao, S. Su, and B. Thomas, *Dilepton Signals in the Inert Doublet Model*, *Phys. Rev.* **D81** (2010) 035003, [[0909.3094](#)].
- [67] **ATLAS Collaboration** Collaboration, *Search for electroweak production of supersymmetric particles in the two and three lepton final state at $\sqrt{s} = 13$ TeV with the ATLAS detector*, Tech. Rep. ATLAS-CONF-2017-039, CERN, Geneva, Jun, 2017.
- [68] **CMS Collaboration** Collaboration, *Search for selectrons and smuons at $\sqrt{s} = 13$ TeV*, Tech. Rep. CMS-PAS-SUS-17-009, CERN, Geneva, 2017.
- [69] **ATLAS** Collaboration, M. Aaboud *et. al.*, *Search for electroweak production of supersymmetric states in scenarios with compressed mass spectra at $\sqrt{s} = 13$ TeV with the ATLAS detector*, *Submitted to: Phys. Rev. D* (2017) [[1712.08119](#)].

- [70] **CMS** Collaboration, A. M. Sirunyan *et. al.*, *Search for new physics in events with two soft oppositely charged leptons and missing transverse momentum in proton-proton collisions at $\sqrt{s} = 13$ TeV*, [1801.01846](#).